International Journal of
INTELLIGENT SYSTEMS AND APPLICATIONS IN ENGINEERING
ISSN:2147-6799 www.ijisae.org Original Research Paper

Binary Classification of Brain Tumor using Early and Late fusion

Shlok Nandurbarkar[1], Abhyuday Singh[1], Himanshu Bute[1], Dr. Nandhini K.[1], Dr. Shilpa Gite[2], Dr. Kumar Rajamani[3]

Submitted: 25/10/2023 **Revised**: 17/12/2023 **Accepted**: 27/12/2023

Abstract: This research delves into the realm of medical imaging and artificial intelligence to enhance the classification of brain tumors, specifically distinguishing between Grade III and Grade IV gliomas. Leveraging the TCGA-GBM dataset, encompassing various image modalities such as Flair, T1, T1ce, T2, and Mask, acquired through magnetic resonance imaging (MRI), the study explores the efficacy of deep learning techniques. Both early and late fusion strategies are employed to amalgamate information from diverse modalities. The convolutional neural network (CNN)-based models exhibit commendable performance in accurately categorizing glioma types, showcasing promise for potential applications in clinical diagnostics.

Keywords**:** *Brain Tumor, CNN, Glioblastoma Multiforme, Binary Classification*

1. Introduction

With gliomas making up 78% of malignant brain tumors, gliomas are the most common type of adult brain tumor [2]. The four grades of gliomas range from Grade I, which is the least aggressive, to Grade IV, which is the most aggressive. The two most aggressive glioma forms are anaplastic astrocytoma (Grade III) and glioblastoma multiforme (Grade IV).In the field of medical imaging, glioma-type classification is a significant problem. This is because on medical images like magnetic resonance imaging (MRI), the two grades of glioma, grade III and grade IV, can be challenging to identify from one another. Deep learning (DL) techniques have lately gained popularity for creating automated systems that can quickly and reliably categorize or diagnose brain tumors [3]. Complex patterns in medical photos that are challenging for human professionals to see can be recognised by DL-based algorithms. In terms of diagnosis and preoperative planning, the outcomes of classification and segmentation employing DL techniques have been highly successful. For instance, it has been demonstrated that DL-based algorithms can accurately classify brain tumors as benign or malignant with accuracies of above 90%. To create DL-based systems that can accurately categorize glioma types, there are still several issues that need to be resolved. One issue is the dearth of sizable databases of expert-labeled glioma images that are publically accessible. Glioma tumors can have a wide range of appearances based on their locations, sizes, and grades, which presents another difficulty.

Grade III and grade IV gliomas can be hard to tell apart on medical images like MRIs, which makes glioma-type classification a serious difficulty in medical imaging. The similarities in appearance between these two grades of glioma and their modest distinctions account for this. Because they can learn to recognize intricate patterns in medical images that are challenging for human professionals to see, deep learning techniques hold promise for the categorization of glioma-type tumors. Brain tumors can be accurately classified as benign or malignant with accuracy rates of over 90% using DL-based algorithms. The absence of substantial, openly accessible datasets of expert-labeled glioma pictures is a difficulty to the development of DL-based systems for glioma-type classification. Glioma tumors can appear in a variety of ways depending on their location, size, and grade, which presents another difficulty. Grade III and grade IV gliomas can be accurately identified in brain tumors by DL-based algorithms when they have been adequately trained and validated. Clinicians can use this information to make wiser decisions about patient care. Patients with grade IV gliomas, for instance, which are more aggressive and have a worse prognosis, may benefit more from intensive treatment options including surgery and radiation therapy. It's critical to keep in mind that DL-based systems cannot take the role of experienced human judgment. For patients to receive the greatest care, DL-based solutions should be used in conjunction with the expertise of seasoned professionals. Overall, using deep learning approaches to create automated glioma-type classification systems is a promising strategy. Such systems could support doctors in making wiser decisions on patient care, resulting in better patient outcome.

[1]*Department of Artificial Intelligence and Machine Learning, Symbiosis Institute of Technology, Symbiosis Internation (Deemed University), Pune, India.*
[2]*Symbiosis Centre for Applied AI, Symbiosis International (Deemed University), Pune, India.*
[3]*Senior Manager Algorithms, KLA-Tencor, India.*
Emails: shlok4112000@gmail.com, abhyuday.singh.mtech2023@sitpune.edu.in, himanshubute.work@gmail.com, nandhinik@gmail.com, shilpagite15@gmail.com, , kumarthirunellai.rajamani@kla-tencor.com.
Corresponding Author: Dr. K. Nandhini.

The DL model can categorize brain tumors into grade iii and grade iv gliomas with excellent accuracy if it is properly trained and validated. Clinicians may be able to make better decisions about patient treatment as a result. It's crucial to remember that dl-based systems cannot take the role of human expertise. To guarantee that patients receive the best care possible, dl-based systems should be used in conjunction with practitioners' knowledge.

2. Related Work

In [1], a new method was developed for predicting the prognosis of brain tumors in adults and children. The method combines two types of data: images of the tumor and information about the tumor's genes. The new method is more accurate than previous methods that used only one type of data. The researchers also showed that the new method can be used to predict the prognosis of rare brain tumors in children.

In [2], a new approach to brain tumor detection and classification using a fine-tuned CNN was developed. Their CNN achieved an accuracy of 95% in detecting brain tumors and 93%in classifying brain tumors as benign or malignant. This suggests that their CNN is an effective tool for brain tumor detection and classification.

In [3], The study proposed a new approach to brain tumor detection using an ensemble of deep learning models. They trained their ensemble of models on a dataset of over 2,000 brain tumor images, and it achieved an accuracy of 98% in detecting brain tumors. The authors concluded that their ensemble of deep learning models is an effective tool for brain tumor detection.

In [4], The paper proposed a new decision support system for multimodal brain tumor classification using deep learning. The system achieved an accuracy of 95% in classifying brain tumors into four types, which is higher than the accuracy of human radiologists. The system can help radiologists classify brain tumors more accurately and efficiently, leading to better patient care.

In [19-22], other brain related diseases are being explored with advanced ML/DL approaches.

3. Dataset Description

The Centre of Cancer Genomics at the National Cancer Institute in the United States provided the TCGA-GBM dataset, which we used [1]. Images of glioblastoma multiforme (GBM) tumors from more than 500 patients may be found in this dataset. The photos were not taken as part of a clinical trial or a controlled research study; rather, they were taken as part of ordinary medical care. The dataset includes the following image modalities: Flair, T1, T1ce, T2 and Mask These photos will be used to train a deep-learning model that will categorize GBM tumors according to their grade.

Because the TCGA dataset contains a sizable and comprehensive collection of GBM tumors, we decided to use it. Additionally, the dataset includes photographs from numerous international websites, which will aid in the generalization of our model to new data. We are thrilled to use the TCGA dataset to create a deep-learning model that will aid physicians in more accurately identifying and grading GBM tumors.

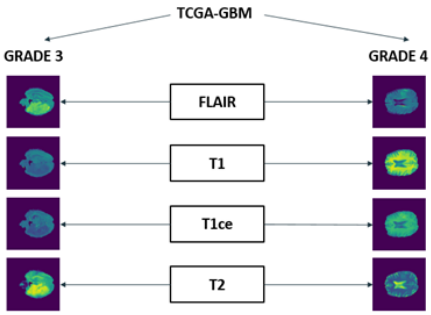

Fig. 1. Dataset Overview

A. Data Volume Used

Our model has been trained on 1413 image samples of each modality i.e flair, t1, t2, t1ce, in GRADE 3 type and on 1443 image samples of each modality in GRADE 4.

All the modalities within each grade type have data for the same patient IDs taken over certain period of time. Also every image in each modalities corresponds to the image in other modalities in same grade type. In other words, say first few images in all modalities belong to patient A and next few images in all modalities belong to patient B and so on. Although patient IDs across GRADE 3 and GRADE 4 are completely different.

We also have the ‘mask’ data for both grade types which further provides us with the scope for segmentation application for tumor area detection within the image. But for the sake of this study we have limited us to the classification of grade types only.

TABLE I. DATA VOLUME

Grade Type	Modality	No. Of Samples
GRADE 3	Flair	1413
	T1	
	T2	
	T1ce	
GRADE 4	Flair	1443
	T1	
	T2	
	T1ce	

B. Data Pre-processing

The original data acquired had data for all the patients that were examined for possibility of having any glioma (brain tumor). Thus many of the images in the dataset belonged to the patient IDs that were not detected with any presence of glioma. Therefore, such images served no purpose in this study and thus have been trimmed out of the dataset leaving us with the volume of data as mentioned in the previous section.

4. Methodology

The TCGA image data will be divided into training and test sets. This is a typical split for machine learning datasets, and it makes sure we have enough information to build our model and assess how well it works. We made an 80% and 20% split for training and testing data respectively.

Since this study aims to find out the best performing model across all possible combinations of modality and the best performing deep learning model:

- Firstly, we trained a CNN model for each modality i.e. flair, t1, t2, t1ce one by one and analyze the performance for classification using each modality.
- Then we created all possible combinations of two modalities and analyzed the performance for classification using each combination. The combinations were flair + t1, flair + t2, flair + t1ce, t1 + t2, t1 + t1ce, t2 + t1ce.
- Next, we created all possible combinations of three modalities and analyzed the performance for classification using each combination. The combinations were flair + t1 + t2, flair + t1 + t1ce, t1 + t2 +t1ce.
- Finally, we combined all four modalities and analyzed the performance for classification between GRADE 3 and GRADE 4 types.

An early fusion model and a late fusion model will both be trained for all modality combination tasks. The features from all modalities are concatenated in an early fusion model before being supplied into the model. A model processes the characteristics from each modality independently in a late fusion model before combining the results of the models. A general CNN model with a ReLU activation function will be employed. ReLU is a well-liked activation function for CNNs, and they are excellent in image classification tasks. The model will be trained for 20 epochs, 32 batch size.

The test dataset will be used to evaluate the models. This will enable us to predict how effectively the models will function with fresh data.

C. Early Fusion

In this technique we first fuse all the different modalities and then apply model over this fused data for feature extraction and then perform classification.

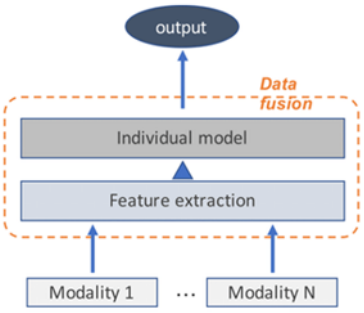

Fig. 2. Early Fusion

D. Late Fusion

In this technique we apply individual model over each modality and extract their features separately and then fuse them for classification.

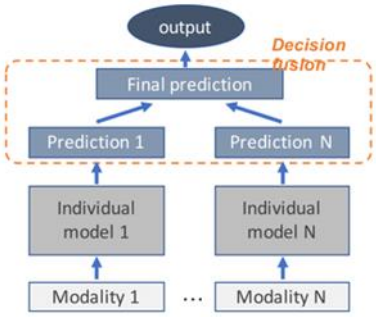

Fig. 3. Late Fusion

Thus, using these two techniques, the results could be compared and optimum technique could be chosen.

E. Training Over Single Modality

For Single Modality Training we took each modality one after one and then first combined GRADE-3 and GRADE-4 data of each modality along with their respective labels. Then the 80% of this set was trained on a simple CNN architecture for 20 epochs and batch size of 32. This process was repeated for all the modalities. The results of each modality and the CNN architecture have been described in coming sections.

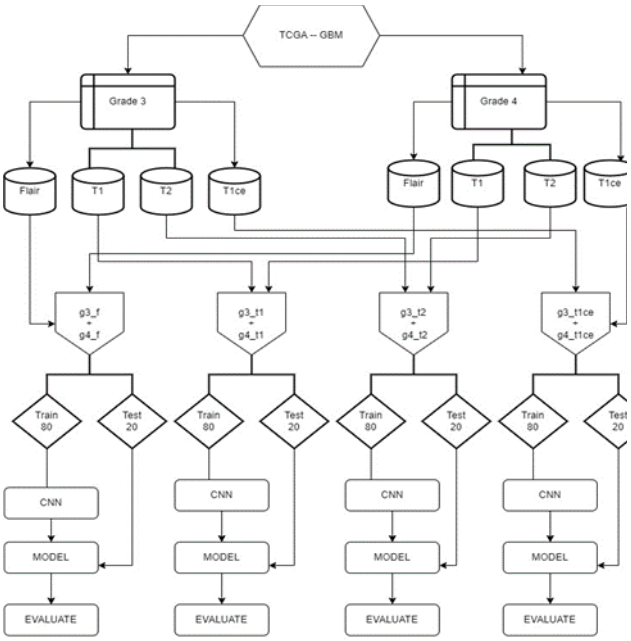

Fig. 4. Training Single Modality

F. Process of Fusing Modalities for Early Fusion

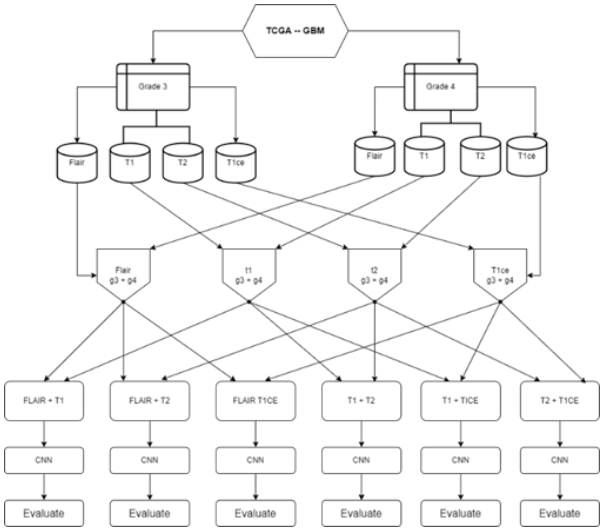

Fig. 5. Training Early Fusion for two modalities

Fusing Two Modalities: Similar as for training single modality we first combined GRADE-3 and GRADE-4 data of each modality along with their respective labels. Then all the possible combinations of two modalities i.e., *flair+t1, flair+t2, flair+t1ce, t1+t2, t1+t1ce, t2+t1ce* are created by concatenating original modalities. This each of the concatenated or fused combinations are trained using the CNN model, hence creating an early fusion result for two modalities.

Fusing Three Modalities: Same process as double fusion, only difference is the combinations to be made and they are *flair+t1+t2, flair+t1+t1ce, flair+t2_t1ce, t1+t2+t1ce*. All these modalities are created using concatenating original modalities.

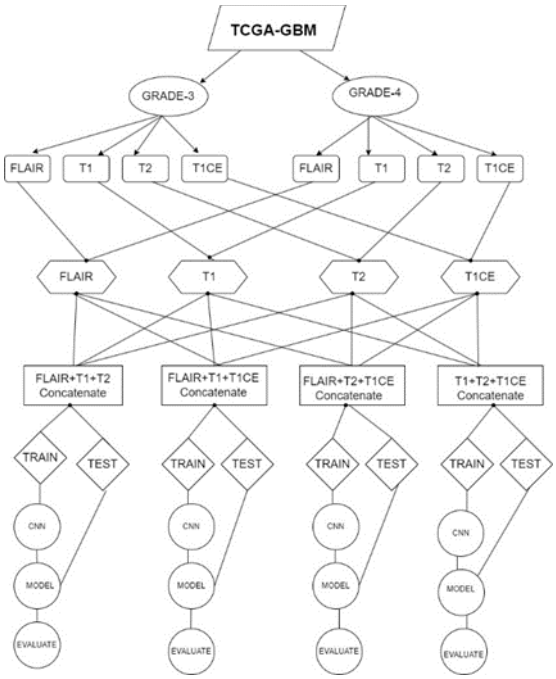

Fig. 6. Training Early Fusion for three modalities

Four Fusion: Same process as double and triple fusion but only we have one combination, flair*+t1+t2+t1ce* which is made by concatenating all four original modalities and then training this with a CNN model.

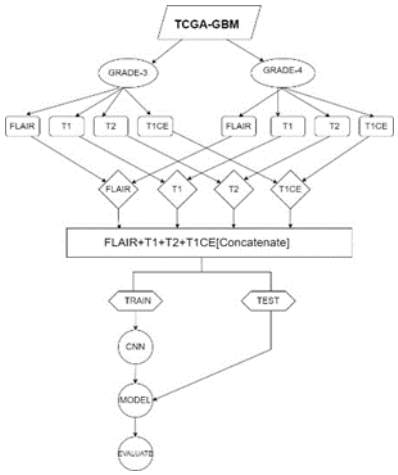

Fig. 7. Training Early Fusion for four modalities

G. Process of Fusing Modalities for Late Fusion

First, as before we combine GRADE-3 and GRADE-4 data for each modality. Then for each modality in all possible combinations of two modalities, three modalities and four modalities, we apply a separate CNN to extract the features then finally the outputs of these CNNs are concatenated into one dense layer and finally the output is acquired using a sigmoid activation function on the output layer, since it is a binary classification.

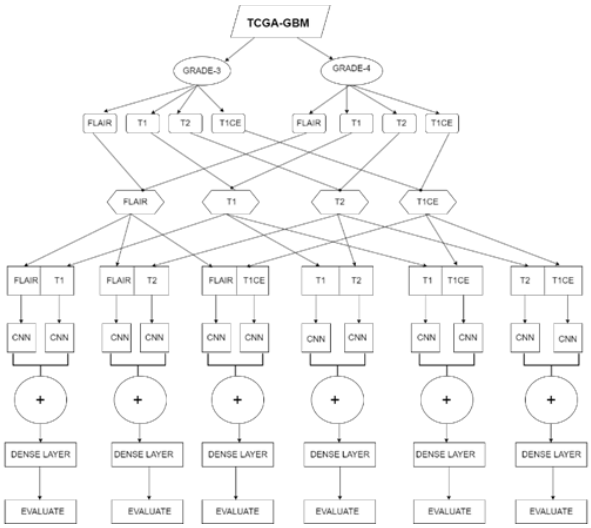

Fig. 8. Training Late Fusion for two modalities

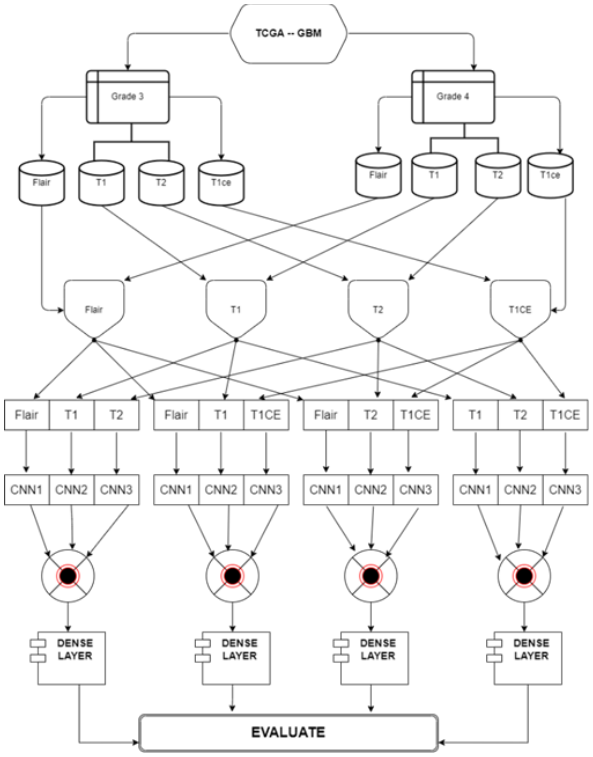

Fig. 9. Training Late Fusion for three modalities

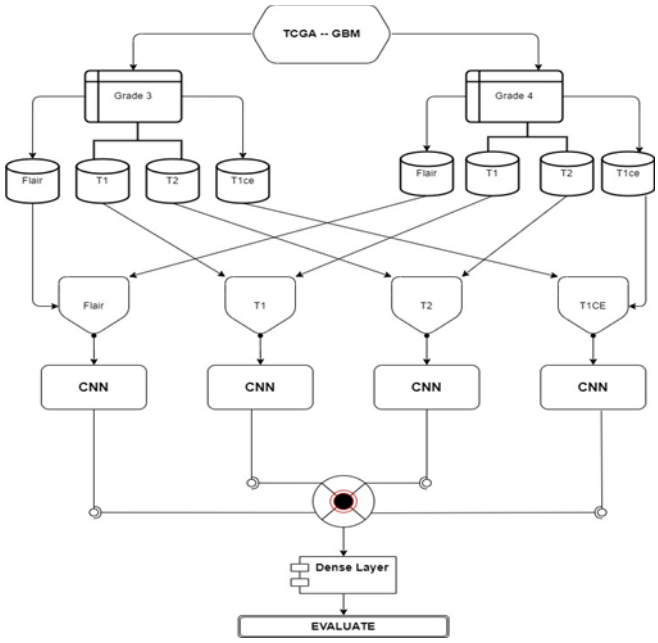

Fig. 10. Training Late Fusion for four modalities

H. The CNN Model

A simple CNN architecture has been used to train all different combinations and both fusion techniques. It was important to keep the architecture as consistent as possible throughout the process to generate unbiased results. Model Definition is shown in figure below:

```
model = Sequential()
model.add(Conv2D(32, (3, 3), activation="relu", input_shape=(224, 224, 3)))
model.add(MaxPooling2D((2, 2)))
model.add(Conv2D(64, (3, 3), activation="relu"))
model.add(MaxPooling2D((2, 2)))
model.add(Conv2D(128, (3, 3), activation="relu"))
model.add(MaxPooling2D((2, 2)))
model.add(Flatten())
model.add(Dense(128, activation="relu"))
model.add(Dense(1, activation="sigmoid"))  # 1 neuron for binary classification
```

Fig. 11. Model Definition

Single architecture and Early Fusion:

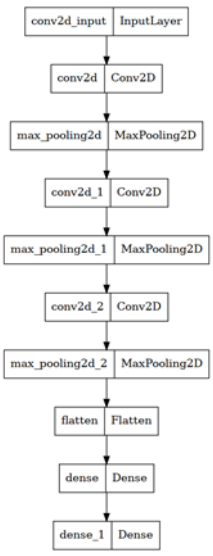

Fig. 12. CNN architecture for single modality and Early Fusion

For Single modality and Early Fusion similar architecture has been used. While for late fusion, for all two, three and four modality combinations the architecture is different.

Two modalities in Late Fusion:

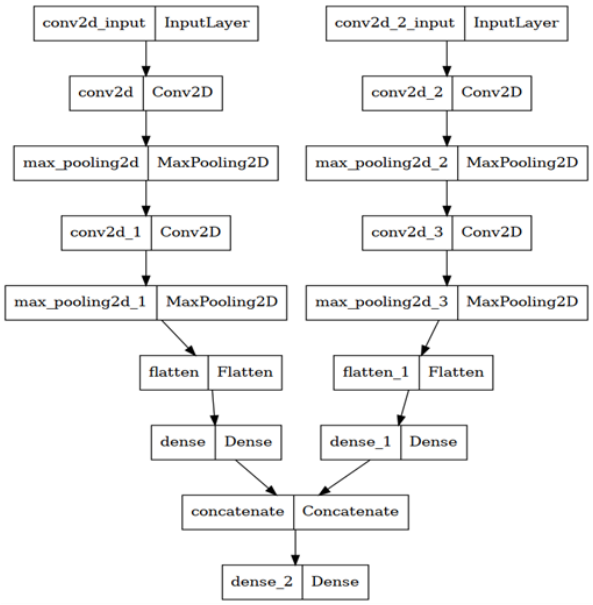

Fig. 13. CNN architecture for Two modalities in Late Fusion

Three modalities in Late Fusion:

Fig. 14. CNN architecture for Three modalities in Late Fusion

Four modalities in Late Fusion:

Fig. 15. CNN architecture for Four modalities in Late Fusion

5. Results

Following are the results obtained after performing all the process as mentioned in 'Methodology' section.

I. Individual Modality

TABLE II. INDIVIDUAL MODALITY RESULTS

Modality	Metrics			
	Accuracy	***Precision***	***Recall***	***F1 Score***
Flair	**99.65%**	100%	99.30%	99.65%
T1	98.60%	99.64%	97.57%	98.60%
T2	99.12%	99.65%	98.61%	99.13%
T1ce	97.55%	97.57%	97.57%	97.57%

Flair:

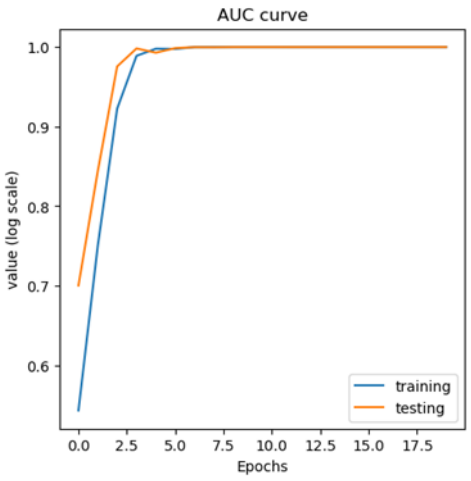

Fig. 16. AUC Curve for Flair

T1:

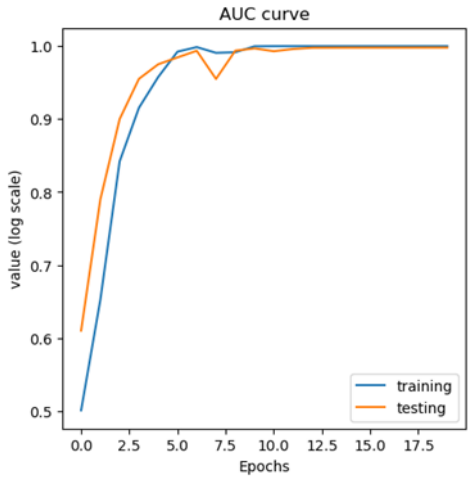

Fig. 17. AUC Curve for Flair

T2:

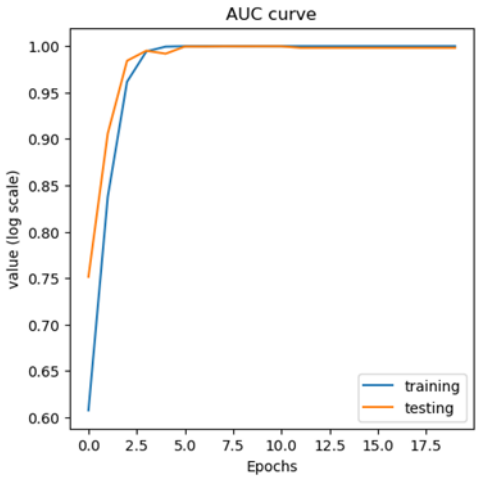

Fig. 18. AUC Curve for Flair

T1ce:

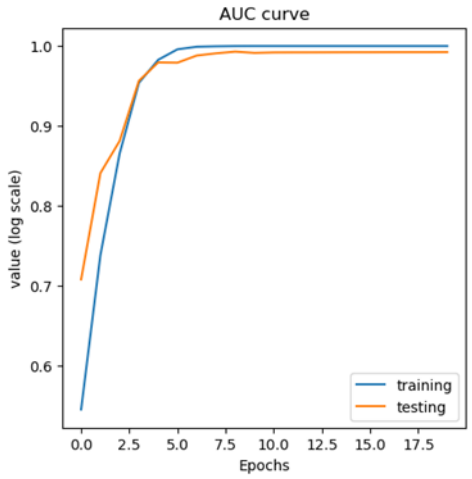

Fig. 19. AUC Curve for Flair

J. Early Fusion

TABLE III. EARLY FUSION RESULTS OF TWO MODALITIES

Modality Combination	**Metrics**			
	Accuracy	***Precision***	***Recall***	***F1 Score***
Flair+T1	99.47%	98.97%	100%	99.48 %
Flair+T2	99.47%	99.65%	99.30 %	99.48 %
Flair+T1ce	99.30%	98.96%	99.65 %	99.31 %
T1+T2	**99.65%**	99.31%	100%	99.65 %
T1+T1ce	**99.65%**	99.65%	99.65 %	99.65 %
T2+T1ce	98.95%	97.96%	100%	98.97 %

Flair + T1:

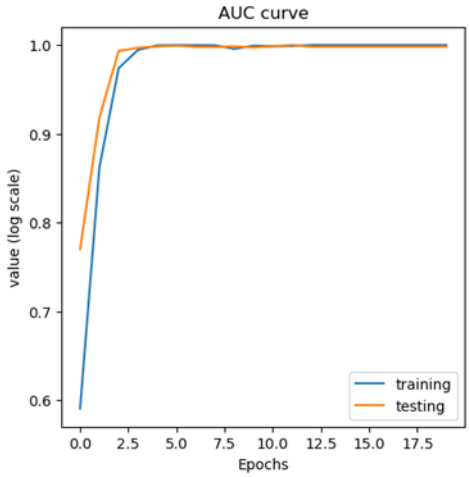

Fig. 20. AUC Curve for Flair + T1

Flair + T2:

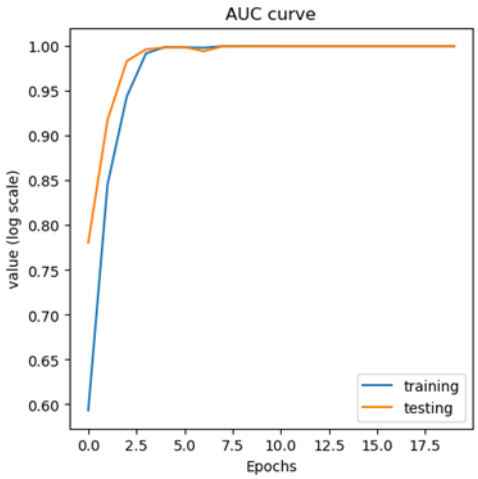

Fig. 21. AUC Curve for Flair + T2

Flair + T1ce:

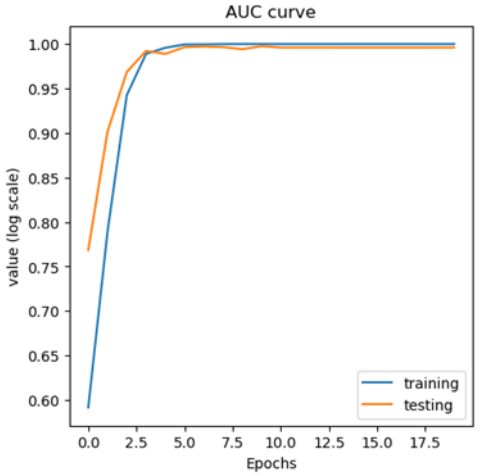

Fig. 22. AUC Curve for Flair + T1ce

T1 + T2:

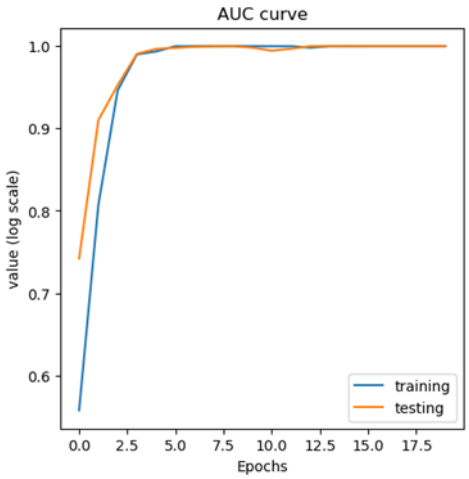

Fig. 23. AUC Curve for T1 + T2

T1 + T1ce:

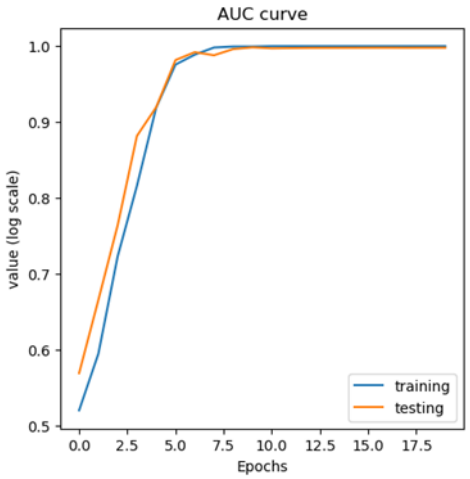

Fig. 24. AUC Curve for T1 + T1ce

T2 + T1ce:

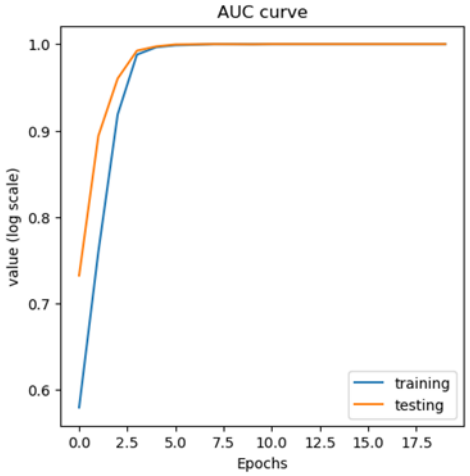

Fig. 25. AUC Curve for T2 + T1ce

TABLE IV. EARLY FUSION RESULTS OF THREE MODALITIES

Modality Combination	**Metrics**			
	Accuracy	***Precision***	***Recall***	***F1 Score***
Flair+T1+T2	99.47%	100%	98.96 %	99.47 %
Flair+T1+T1ce	99.12%	98.96%	99.30 %	99.13 %
Flair+T2+T1ce	99.30%	99.65%	98.96 %	99.30 %
T1+T2+T1ce	**99.65%**	99.31%	100%	99.65 %

Flair + T1 + T2:

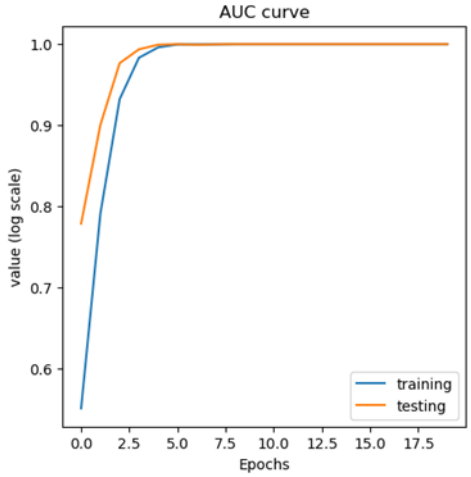

Fig. 26. AUC Curve for Flair + T1 + T2

Flair + T1 + T1ce:

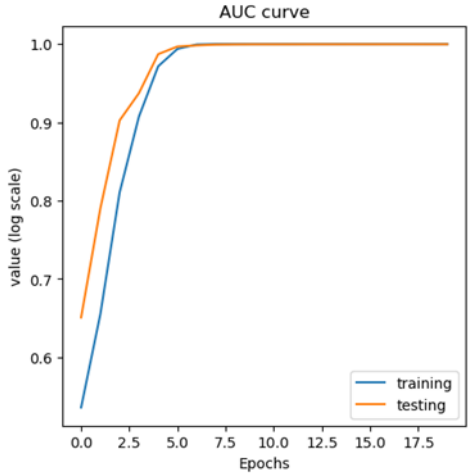

Fig. 27. AUC Curve for Flair + T1 + T1ce

Flair + T2 + T1ce:

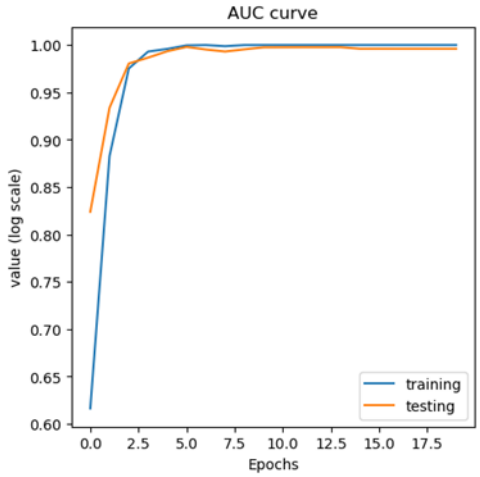

Fig. 28. AUC Curve for Flair + T2 + T1ce

T1 + T2 + T1ce:

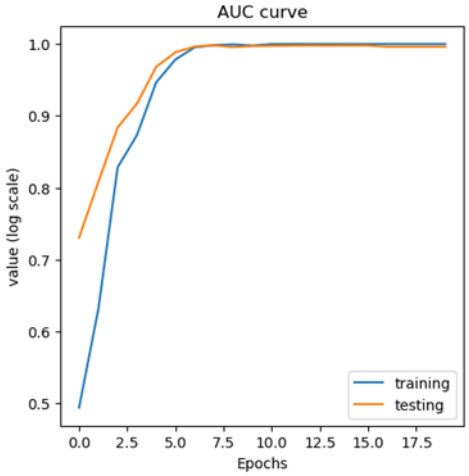

Fig. 29. AUC Curve for T1 + T2 + T1ce

TABLE V. EARLY FUSION RESULTS OF ALL MODALITIES

Modality Combination	Metrics			
	Accuracy	***Precision***	***Recall***	***F1 Score***
Flair+T1+T2+T1ce	99.12%	98.63%	99.65 %	99.13 %

Flair + T1 + T2 + T1ce:

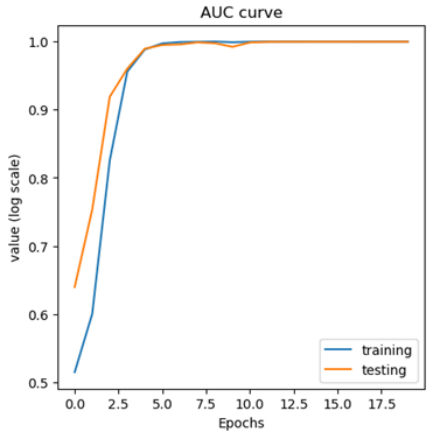

Fig. 30. AUC Curve for Flair+T1+T2+T1ce

K. Late Fusion

TABLE VI. LATE FUSION RESULTS OF TWO MODALITIES

Modality Combination	Metrics			
	Accuracy	***Precision***	***Recall***	***F1 Score***
Flair+T1	**99.65%**	100%	99.30 %	99.65 %

Flair+T2	**99.65%**	100%	99.30 %	99.65 %
Flair+T1ce	98.77%	99.64%	97.92 %	98.77 %
T1+T2	99.12%	98.96%	99.30 %	99.13 %
T1+T1ce	98.77%	99.30%	98.26 %	98.78 %
T2+T1ce	99.30%	99.30%	99.30 %	99.30 %

Flair + T1:

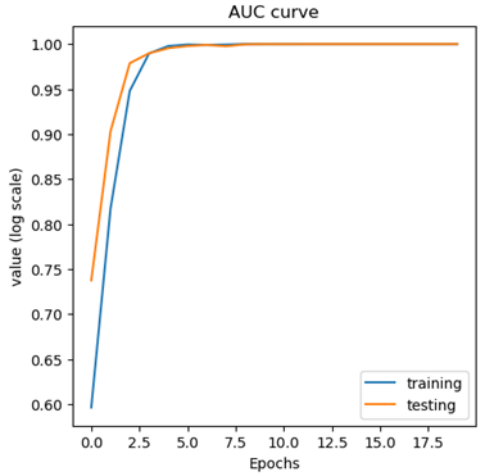

Fig. 31. AUC Curve for Flair + T1

Flair + T2:

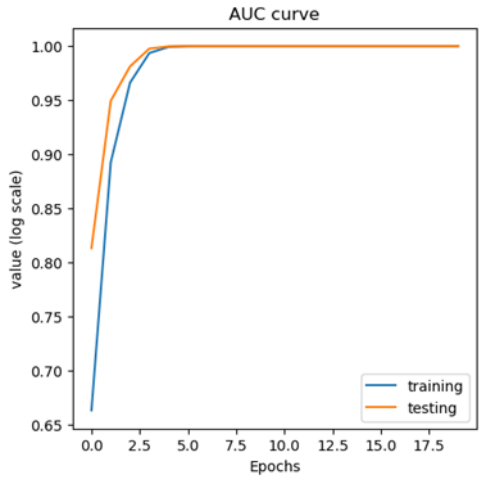

Fig. 32. AUC Curve for Flair + T2

Flair + T1ce:

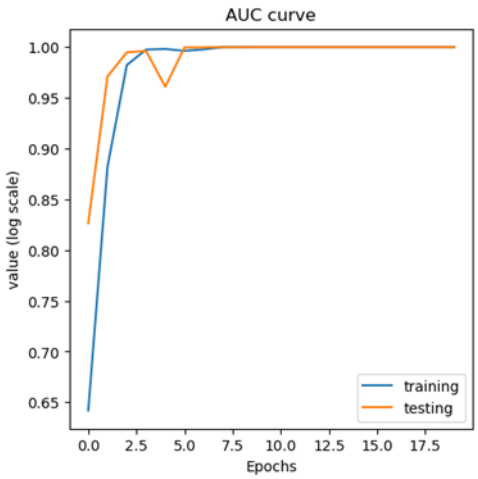

Fig. 33. AUC Curve for Flair + T1ce

T1 + T2:

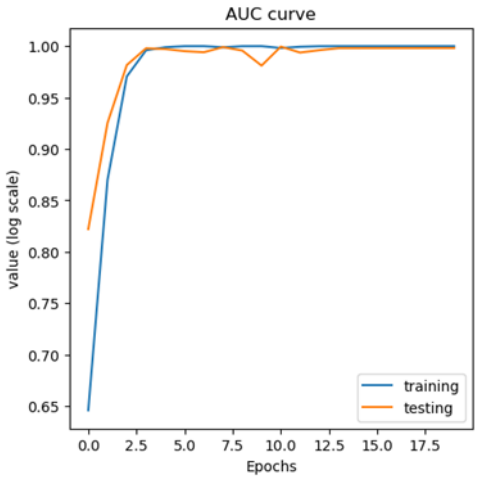

Fig. 34. AUC Curve for T1 + T2

T1 + T1ce:

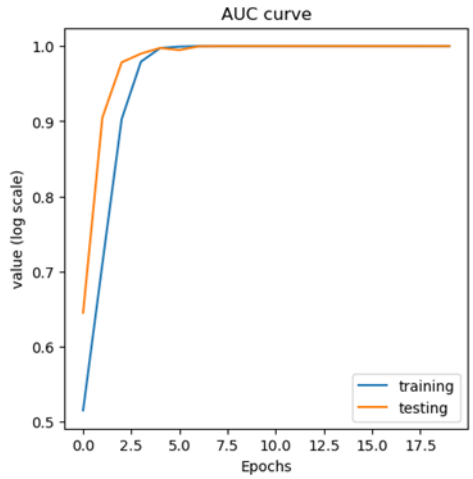

Fig. 35. AUC Curve for T1 + T1ce

T2 + T1ce:

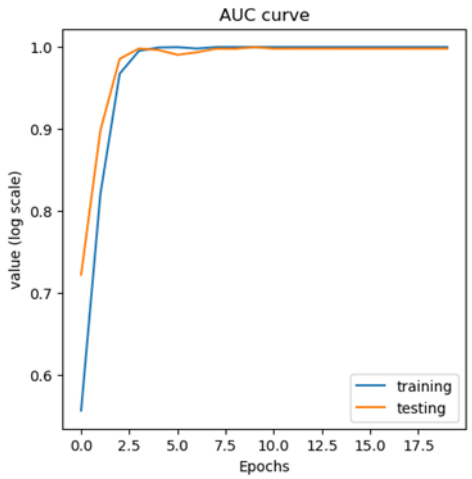

Fig. 36. AUC Curve for T2 + T1ce

TABLE VII. LATE FUSION RESULTS OF THREE MODALITIES

Modality Combination	Metrics			
	Accuracy	***Precision***	***Recall***	***F1 Score***
Flair+T1+T2	**99.47%**	99.65%	99.30 %	99.48 %
Flair+T1+T1ce	**99.47%**	100%	98.96 %	99.47 %
Flair+T2+T1ce	**99.47%**	99.65%	99.30 %	99.48 %
T1+T2+T1ce	99.30%	99.30%	99.30 %	99.30 %

Flair + T1 + T2:

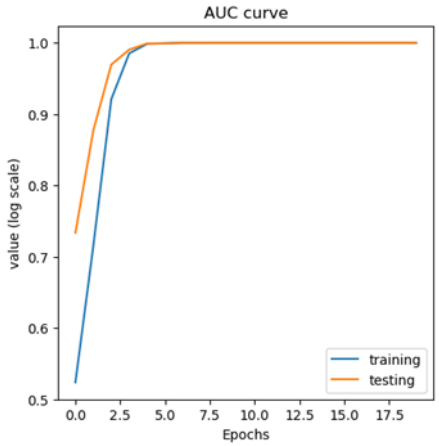

Fig. 37. AUC Curve for Flair + T1 + T2

Flair + T1 + T1ce:

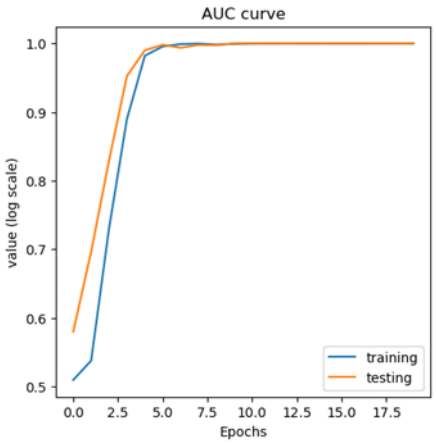

Fig. 38. AUC Curve for Flair + T1 + T1ce

Flair + T2 + T1ce:

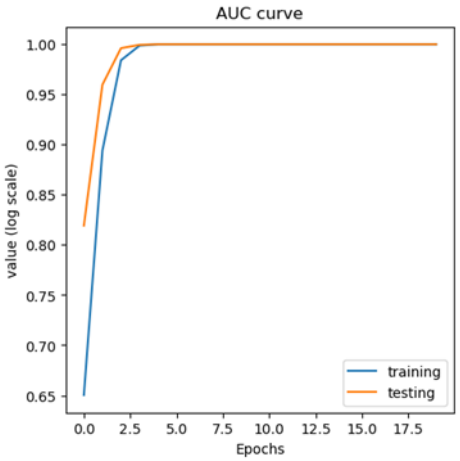

Fig. 39. AUC Curve for Flair + T2 + T1ce

T1 + T2 + T1ce:

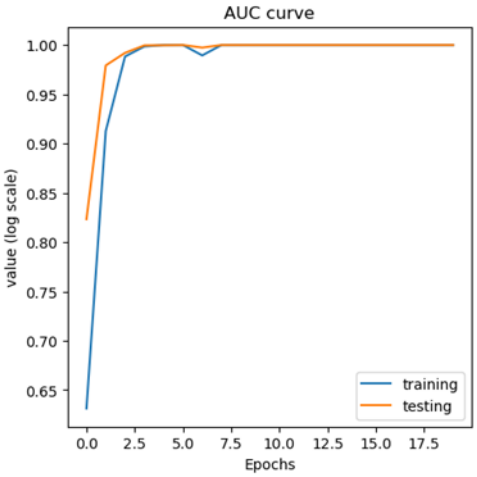

Fig. 40. AUC Curve for T1 + T2 + T1ce

TABLE VIII. LATE FUSION RESULTS OF ALL MODALITIES

Modality Combination	Metrics			
	Accuracy	***Precision***	***Recall***	***F1 Score***
Flair+T1+T2+T1ce	99.30%	99.65%	98.96 %	99.30 %

Flair + T1 + T2 + T1ce:

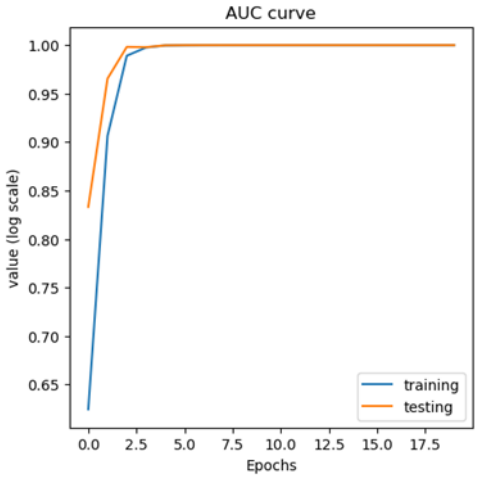

Fig. 41. AUC Curve for Flair+T1+T2+T1c

6. Conclusion

Our investigation successfully navigates the intricate landscape of brain tumor classification using advanced technologies. Individual modalities and their amalgamations through early and late fusion methodologies were systematically evaluated. The findings underscore the models' high accuracy, precision, recall, and F1 scores across various configurations. While both early and late fusion proved effective, early fusion demonstrated a slight advantage. This study not only contributes insights into optimal fusion strategies but also presents a noteworthy advancement in leveraging deep learning for improved brain tumor diagnostics. The implications extend beyond technology, aiming to enhance the precision and efficacy of clinical decision-making in neuro-oncology.

ACKNOWLEDGMENT

We would like to express gratitude to Symbiosis Institute of Technology, Pune, India, for providing the necessary infrastructure and support for the successful completion of this Deep Learning project. Special thanks are extended to Dr. Shilpa Gite and Dr. Nandhini K. for invaluable guidance and mentorship throughout the project.

References

[1] Steyaert, S., Qiu, Y.L., Zheng, Y. et al. Multimodal deep learning to predict prognosis in adult and pediatric brain tumors. Commun Med 3, 44 (2023). https://doi.org/10.1038/s43856-023-00276-y

[2] Asiri AA, Shaf A, Ali T, Aamir M, Irfan M, Alqahtani S, Mehdar KM, Halawani HT, Alghamdi AH, Alshamrani AFA, Alqhtani SM. Brain Tumor Detection and Classification Using Fine-Tuned CNN with ResNet50 and U-Net Model: A Study on TCGA-LGG and TCIA Dataset for MRI Applications. Life (Basel). 2023 Jun 26;13(7):1449. doi: 10.3390/life13071449. PMID: 37511824; PMCID: PMC10381218

[3] Alsubai S, Khan HU, Alqahtani A, Sha M, Abbas S, Mohammad UG. Ensemble deep learning for brain tumor detection. Front Comput Neurosci. 2022 Sep 2;16:1005617. doi: 10.3389/fncom.2022.1005617. PMID: 36118133; PMCID: PMC9480978.

[4] Sharif, M.I., Khan, M.A., Alhussein, M. et al. A decision support system for multimodal brain tumor classification using deep learning. Complex Intell. Syst. 8, 3007–3020 (2022). https://doi.org/10.1007/s40747-021-00321-0

[5] H. A. Hafeez et al., "A CNN-Model to Classify Low-Grade and High-Grade Glioma From MRI Images," in IEEE Access, vol. 11, pp. 46283-46296, 2023, doi: 10.1109/ACCESS.2023.3273487.

[6] Taher Fatma, Shoaib Mohamed R., Emara Heba M., Abdelwahab Khaled M., Abd El-Samie Fathi E., Haweel MohammadT.-Efficient framework for brain tumor detection using different deep learning techniques.

[7] Dwivedi, Shubham, et al. "Multimodal fusion-based deep learning network for effective diagnosis of Alzheimer's disease." *IEEE MultiMedia* 29.2 (2022): 45-55.

[8] Alorf, Abdulaziz, and Muhammad Usman Ghani Khan. "Multi-label classification of Alzheimer's disease stages from resting-state fMRI-based correlation connectivity data and deep learning." *Computers in Biology and Medicine* 151 (2022): 106240.

[9] Shi, Jun, et al. "Multimodal neuroimaging feature learning with multimodal stacked deep polynomial networks for diagnosis of Alzheimer's disease." *IEEE journal of biomedical and health informatics* 22.1 (2017): 173-183.

[10] Efficient framework for brain tumor detection using different deep learning techniquesZou, Ying, et al. "A new prediction model for lateral cervical lymph node metastasis in patients with papillary thyroid carcinoma:

based on dual-energy CT." *European Journal of Radiology* 145 (2021): 110060.

[11] Chen, Xiangmeng, et al. "A CT-based deep learning model for subsolid pulmonary nodules to distinguish minimally invasive adenocarcinoma and invasive adenocarcinoma." *European Journal of Radiology* 145 (2021): 110041.

[12] Kriza C, Amenta V, Zenié A, Panidis D, Chassaigne H, Urbán P, Holzwarth U, Sauer AV, Reina V, Griesinger CB. Artificial intelligence for imaging-based COVID-19 detection: Systematic review comparing added value of AI versus human readers. Eur J Radiol. 2021 Dec;145:110028. doi: 10.1016/j.ejrad.2021.110028. Epub 2021 Nov 16. PMID: 34839214; PMCID: PMC8594127.

[13] Tolonen A, Pakarinen T, Sassi A, Kyttä J, Cancino W, Rinta-Kiikka I, Pertuz S, Arponen O. Methodology, clinical applications, and future directions of body composition analysis using computed tomography (CT) images: A review. Eur J Radiol. 2021 Dec;145:109943. doi: 10.1016/j.ejrad.2021.109943. Epub 2021 Aug 30. PMID: 34839215.

[14] van Oostenbrugge TJ, Spenkelink IM, Bokacheva L, Rusinek H, van Amerongen MJ, Langenhuijsen JF, Mulders PFA, Fütterer JJ. Kidney tumor diffusion-weighted magnetic resonance imaging derived ADC histogram parameters combined with patient characteristics and tumor volume to discriminate oncocytoma from renal cell carcinoma. Eur J Radiol. 2021 Dec;145:110013. doi: 10.1016/j.ejrad.2021.110013. Epub 2021 Oct 30. PMID: 34768055.

[15] Chandarana H, Pisuchpen N, Krieger R, Dane B, Mikheev A, Feng Y, Kambadakone A, Rusinek H. Association of body composition parameters measured on CT with risk of hospitalization in patients with Covid-19. Eur J Radiol. 2021 Dec;145:110031. doi: 10.1016/j.ejrad.2021.110031. Epub 2021 Nov 15. PMID: 34801878; PMCID: PMC8592118.

[16] Alom, Md Zahangir, et al. "Recurrent residual convolutional neural network based on u-net (r2u-net) for medical image segmentation." *arXiv preprint arXiv:1802.06955* (2018).

[17] Zhou, Zongwei, et al. "Unet++: Redesigning skip connections to exploit multiscale features in image segmentation." *IEEE transactions on medical imaging* 39.6 (2019): 1856-1867.

[18] Özkaraca, Osman, et al. "Multiple Brain Tumor Classification with Dense CNN Architecture Using Brain MRI Images." *Life* 13.2 (2023): 349.

[19] Tavse, S.; Varadarajan, V.; Bachute, M.; Gite, S.; Kotecha, K. A Systematic Literature Review on Applications of GAN-Synthesized Images for Brain MRI. *Future Internet* **2022**, *14*, 351. https://doi.org/10.3390/fi14120351

[20] Deshpande, N. M., Gite, S., Pradhan, B., Assiri, M. E. (2022). Explainable Artificial Intelligence–A New Step towards the Trust in Medical Diagnosis with AI Frameworks: A Review. *CMES-Computer Modeling in Engineering & Sciences, 133(3)*, 843–872.

[21] V. Jain, O. Nankar, D. J. Jerrish, S. Gite, S. Patil and K. Kotecha, "A Novel AI-Based System for Detection and Severity Prediction of Dementia Using MRI," in *IEEE Access*, vol. 9, pp. 154324-154346, 2021, doi: 10.1109/ACCESS.2021.3127394.

[22] Salunkhe, S.; Bachute, M.; Gite, S.; Vyas, N.; Khanna, S.; Modi, K.; Katpatal, C.; Kotecha, K. Classification of Alzheimer's Disease Patients Using Texture Analysis and Machine Learning. *Appl. Syst. Innov.* 2021, *4*, 49. https://doi.org/10.3390/asi4030049